Volume 1 | Number 1 | Jan 2013 | Pages 1–100

Journal of
Materials Chemistry A

Materials for energy and sustainability
www.rsc.org/materialsA

Li⁺

ROYAL SOCIETY
OF CHEMISTRY

ROYAL SOCIETY
OF CHEMISTRY

www.rsc.org/materialsA

Journal Name

ARTICLE

Multi-Nanoparticle Model Simulations of the Porosity Effect on Sintering Processes in Ni/YSZ and Ni/ScSZ by Molecular Dynamics Method

Jingxiang Xu,[a] Shandan Bai,[b] Yuji Higuchi,[a] Nobuki Ozawa,[a] Kazuhisa Sato,[c] Toshiyuki Hashida,[c] and Momoji Kubo*[a]

Understanding the sintering mechanism in porous anodes is necessary for developing durable anodes suitable for use in solid oxide fuel cells. A multi-nanoparticle sintering simulation method based on molecular dynamics (MD) calculation was developed for this purpose [J. Xu et al., *J. Phys. Chem. C*, 2013, **117**, 9663-9672]. The method can calculate the effect of the porous structure properties, such as porosity and framework structure, on the sintering, unlike previous sintering simulations with conventional nanoparticle models. We revealed that in a Ni/YSZ porous anode, the YSZ nanoparticle framework suppresses sintering of Ni nanoparticles by disrupting the growth of the neck between two Ni nanoparticles. In this paper, we used our method to reveal the effect of ceramic type on the sintering processes. We investigated the difference between the sintering and degradation processes in Ni/YSZ and Ni/ScSZ anodes. In the simulation, the degree of sintering of the Ni nanoparticles in Ni/ScSZ was smaller than that in Ni/YSZ. The stronger adhesion of Ni to ScSZ nanoparticles than to YSZ nanoparticles prevented the Ni nanoparticles from approaching each other in the Ni/ScSZ anode, inhibiting sintering. Our multi-nanoparticle sintering MD simulations revealed the different sintering processes for Ni nanoparticles in Ni/YSZ and Ni/ScSZ anodes. We also investigated the effect of sintering on degradation. The hydrogen adsorption sites and electrochemical reaction sites of the hydrogen oxidation decreased as the degree of sintering increased. A low degradation of the Ni/ScSZ anode relative to that of the Ni/YSZ anode was observed. Furthermore, we showed the effect of porosity on degradation induced by sintering in Ni/YSZ and Ni/ScSZ, and found an optimal porosity. These findings cannot be obtained by conventional two- or three-nanoparticle sintering MD simulations. Our multi-nanoparticle sintering simulation method is useful for revealing the types of ceramic suitable for inhibiting sintering and degradation in anodes, and can be used to design durable anodes.

1. Introduction

Solid oxide fuel cells (SOFCs), which convert chemical energy to electrical energy, are expected to be used for power generation owing to their low pollutant emissions, efficient energy production, and low cost.[1–4] Nickel and yttria-stabilized zirconia (Ni/YSZ) cermet is the most widely used SOFC anode material because of its low cost and good electrocatalytic oxidation properties at high operating temperatures.[2] However, sintering of Ni nanoparticles occurs during long-term operation because Ni catalyst nanoparticles have a relatively low melting temperature and show a high surface mobility at high operating temperatures.[2] Several studies have reported

the coalescence and densification of Ni nanoparticles caused by the sintering of Ni nanoparticles in Ni/YSZ anodes.[5,6] Sintering decreases the number of hydrogen adsorption sites and the number of electrochemical reaction sites for hydrogen oxidation.[6] Moreover, the coalescence induced by sintering destroys the path for ionic conduction and decreases electrical conductivity.[7] Thus, to inhibit degradation in Ni-based cermets, sintering must be fully understood.

Scandia-stabilized zirconia (ScSZ) exhibits higher ionic conductivity and anodic reaction activity than YSZ.[8] Sumi et al.[9,10] reported that the output voltage and power density of a Ni/ScSZ anode are higher than those of a Ni/YSZ anode. However, very little is known about the differences in the sintering processes of Ni/YSZ and Ni/ScSZ anodes. Thus, the different degradation mechanisms induced by sintering in Ni/YSZ and Ni/ScSZ are unknown. Although experimental techniques have identified the coalescence and densification of Ni nanoparticles as a consequence of sintering, an atomistic approach is necessary to understand the sintering mechanism because atomic forces are important in the sintering process.

a. *Institute for Materials Research, Tohoku University, 2-1-1 Katahira, Aoba-ku, Sendai 980-8577, Japan. E-mail: momoji@imr.tohoku.ac.jp*
b. *New Industry Creation Hatchery Center, Tohoku University, 6-6-10 Aoba, Aramaki, Aoba-ku, Sendai 980-8579, Japan*
c. *Fracture and Reliability Research Institute, Graduate School of Engineering, Tohoku University, 6-6-11 Aoba, Aramaki, Aoba-ku, Sendai 980-8579, Japan*

Molecular dynamics (MD) simulations are powerful tools to study atomistic behaviors in SOFC.[11–16] Numerous MD simulations have been also used to investigate the sintering mechanism at an atomic scale. We investigated the sintering of two Pd clusters and two Au clusters on the MgO(001) substrate by using MD simulation.[17] We revealed that the sintering proceeds more slowly for Pd clusters than for Au clusters on the MgO(001) substrate. Zhu et al.[18] performed MD simulations of the sintering of two Cu nanoparticles and found that deformation and densification of Cu nanoparticles are induced by large local shear stresses in the necks. Sintering of two TiO_2 nanoparticles was investigated by tracking the shrinkage between the sintered nanoparticles and the surface area.[19,20] However, most previous MD sintering simulations have concentrated on only two- or three-nanoparticle systems.[18–20] Recently, Hawa et al.[21] performed an MD simulation of sintering 40 Si nanoparticles in a straight chain without a substrate. However, the SOFC anode used in the experiment is porous and consists of Ni and ceramic (YSZ and ScSZ) nanoparticles. Scanning-electron microscopy (SEM) has shown that the porosity of a Ni-based ceramic anode has a considerable effect on the sintering,[22,23] and the ceramic nanoparticle framework affects the sintering of the Ni nanoparticles.[15] Therefore, a method of elucidating the effect of the porous structure on sintering is essential for revealing the sintering mechanism and the degradation caused by sintering.

We developed a multi-nanoparticle sintering simulation method based on MD calculation to simulate sintering in the porous structure.[24] Our method takes into account the effects of the porous structure properties, such as porosity, tortuosity, composition, nanoparticle framework, and nanoparticle size, on the sintering. Our developed multi-nanoparticle sintering simulation method is able to reveal the effect of porous structure such as porosity, tortuosity, composition, framework structure, nanoparticle size, etc. on the sintering; in contrast, previous two- or three-nanoparticle sintering simulations cannot. The sintering simulation using the above method was already confirmed to be very effective for reproducing the sintering process in the porous anode.[24] We showed that the three-dimensional YSZ framework suppresses the sintering of Ni nanoparticles in an anode. Furthermore, the effect of the porous structure on the sintering process in a Ni/YSZ anode was also clarified by using the multi-nanoparticle sintering simulation method.[25] However, we investigated the sintering mechanism in only the Ni/YSZ system. Although experimental results showed that the ceramic type affects the sintering process in the porous anode, the effect of the ceramic type on the sintering mechanism and the degradation induced by sintering are still unclear. Understanding the effect of the ceramic type on the sintering mechanism is essential for designing a durable porous anode. Our developed multi-nanoparticle sintering simulation method is able to reveal the effect of ceramic type on the sintering and degradation process in the porous anode, which cannot be revealed by the previous sintering MD model of two- or three-nanoparticles on the substrate. The effect of ceramic type on the sintering and degradation process in the porous anode also cannot be achieved by a wholly quantum mechanical approach because of the system size limitations.

In this study, we elucidated the effect of the ceramic type (for YSZ and ScSZ) on the sintering of Ni nanoparticles and the

degradation induced by sintering in Ni/YSZ and Ni/ScSZ anodes by using our multi-nanoparticle sintering simulation. We introduced our parameterization method for the interaction between Ni and ceramic (YSZ and ScSZ) in the simulation and multi-nanoparticle model. Then, we investigated the sintering processes in the Ni/YSZ and Ni/ScSZ multi-nanoparticle models to reveal the difference in the sintering mechanism and the degradation induced by the sintering. We revealed that the hydrogen adsorption sites and the electrochemical reaction sites of the hydrogen oxidation degrade in Ni/YSZ and Ni/ScSZ porous anodes during the sintering, which could not be shown by previous two- or three-nanoparticle models. Furthermore, the effect of the porosity on the sintering and the degradation induced by sintering in the Ni/YSZ and Ni/ScSZ multi-nanoparticle models are discussed in relation to the theoretical design of a durable anode.

2. Computational Details

The sintering of Ni nanoparticles was simulated by our MD program package, New-Ryudo.[26] In this MD simulator, a Verlet algorithm[27] was used to integrate equations of motion. The MD sintering simulations were executed with a 2.0 fs time-step. The NVT canonical ensemble was performed at a temperature of 1073 K, which is a common SOFC operating temperature. All sintering simulations were run for a total time of 500 ps.

To express the ionic interactions in YSZ and the ScSZ, Born–Mayer–Huggins (BMH) potential[28] was used.

$$U(r_{ij}) = \frac{Z_i Z_j e^2}{r_{ij}} + f_0(b_i + b_j) \times \exp\left(\frac{a_i + a_j - r_{ij}}{b_i + b_j}\right) \quad (1)$$

Here, Z_i is the effective charge of ion i, e is the elementary electric charge, r_{ij} is the interatomic distance, f_0 is a constant to adjust the units, and a_i and b_i are the parameters for the repulsion term and are related to the size and stiffness, respectively. Parameters a_i and b_i were adjusted to reproduce the lattice constants and the thermal expansion coefficients of YSZ and ScSZ. The potential parameters are listed in Table 1.

Morse potential was used to reproduce the Ni-Ni and Ni-ceramic (YSZ and ScSZ) interactions.

$$E(r_{ij}) = D_{ij}\{\exp[-2\beta_{ij}(r_{ij} - r_{ij}^*)] - 2\exp[-\beta_{ij}(r_{ij} - r_{ij}^*)]\} \quad (2)$$

Here, r_{ij} is the interatomic distance, and the parameters D_{ij}, β_{ij}, and r_{ij}^* are related to the bond energy, stiffness, and bond length, respectively. The potential parameters for Ni[29] are presented in Table 2. We used our previous method[24] for

Table 1 BMH potential parameters for YSZ[28] and ScSZ.

Atom	Z_i	a_i/Å	b_i/Å
O	-1.2	1.503	0.075
Zr	+2.4	1.227	0.070
Y	+1.8	1.327	0.070
Sc	+1.8	1.166	0.070

Table 2 Morse potential parameters for Ni.[29]

i-j	D_{ij}/kcal mol^{-1}	β_{ij}/Å^{-1}	R_{ij}^*/Å
Ni-Ni	9.70	1.42	2.78

Table 3 Morse potential parameters for Ni/ceramic (YSZ[24] and Ni/ScSZ)

i-j	D_{ij}/kcal mol^{-1}	β_{ij}/Å^{-1}	R_{ij}^*/Å
Ni-O	31.92	2.35	1.77
Ni-Zr	0.56	1.31	3.80
Ni-Y	0.84	1.08	4.17
Ni-Sc	0.96	1.05	3.96

determining accurate Morse potential parameters to describe the interaction between Ni and the ceramic. In our previous study, we fitted the Morse potential function to the interaction energies between Ni and YSZ as calculated by the DFT.[24] The interatomic potential parameters calculated for Ni and YSZ[24] are presented in Table 3. In this study, we used this method to determine the potential parameters between Ni and ScSZ.

To unravel the effect of ceramic type (YSZ and ScSZ) on the sintering process of nickel nanoparticles, we employed the multi-nanoparticle modeling method developed in our previous study,[24] since the anode is porous structure and the properties of porous structure such as the porosity, tortuosity, composition, nanoparticle framework, nanoparticle size, etc. affect the sintering in the anode.[22,23] In this study, we built Ni/YSZ and Ni/ScSZ multi-nanoparticle models with a desired porosity based on our multi-nanoparticle model.[24] First, five Ni and five ceramic (YSZ and ScSZ) nanoparticles with a diameter of 40 Å were located at similar positions in the Ni/YSZ and Ni/ScSZ simulation cells. The size of simulation cells was 100 × 100 × 100 Å. In the previous studies, NPT ensemble is widely used to build polycrystalline metals.[30–32] In our method, the application of NPT ensemble to the polcycrystalline metals is extended to porous metal/ceramic composite. Thus, we used the NPT ensemble to build metal/ceramic porous model. The initial Ni/ceramic simulation cells were compressed by using the MD simulation in the NPT canonical ensemble under a pressure of 5 GPa until the desired porosity was reached. The periodic boundary condition was imposed in the multi-nanoparticle sintering simulations. All the Ni/YSZ and Ni/ScSZ multi-nanoparticle models were equilibrated at 300 K for a total time of 50 ps after the compression.

3. Results and Discussion

3.1. Sintering Simulation of Ni/YSZ and Ni/ScSZ Multi-nanoparticle Models

To investigate the effect of ceramic type on the sintering mechanism in Ni/YSZ and Ni/ScSZ anodes, we used our multi-nanoparticle sintering simulation method. We built Ni/YSZ and Ni/ScSZ multi-nanoparticle models with a porosity of 0.40, because this is the typical experimental porosity.[33] Figure 1 shows our method for constructing the Ni/ScSZ multi-nanoparticle model. We packed five Ni and five ScSZ nanoparticles into a simulation cell with a size of 100.0 ×100.0 ×100.0 Å (Figure 1(a)). Then, we compressed the simulation cell under a pressure of 5 GPa until the porosity reached 0.40 (Figure 1(b)). The Ni/YSZ multi-nanoparticle model with a porosity of 0.40 was built by using the same method. The sizes of the Ni/YSZ and Ni/ScSZ multi-nanoparticle cells were 86.3 × 83.7 × 78.8 Å and 86.3 × 83.6 × 78.8 Å, respectively. We performed the sintering simulations on the Ni/YSZ and Ni/ScSZ multi-nanoparticle models. Figure 2 shows snapshots of the sintering processes in the Ni/YSZ and Ni/ScSZ multi-nanoparticle models. The initial model of Ni/YSZ, which was stabilized at 300 K, is shown in Figure 2(a). The YSZ nanoparticles were uniformly distributed around the Ni nanoparticles and formed the YSZ framework. After the sintering simulation, a full coalescence of Ni nanoparticles was observed (orange circle in Figure 2(b)). Figure 2(c) is the initial model of Ni/ScSZ multi-nanoparticles similar to that of Ni/YSZ
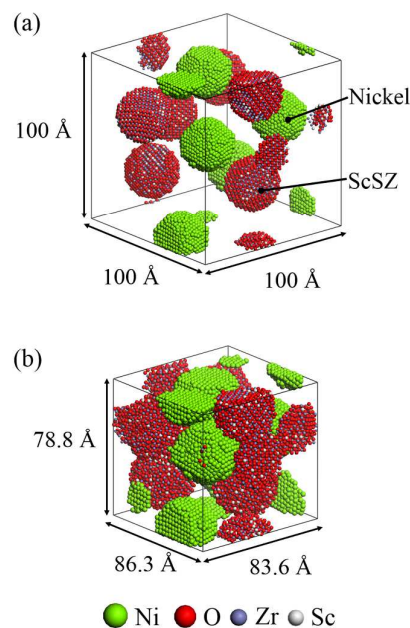

Figure 1. Method for constructing the Ni/ScSZ multi-nanoparticle model. (a) Ni and ScSZ nanoparticles were packed into a 100 × 100 × 100 Å simulation cell at random. (b) The Ni and ScSZ multi-nanoparticle model was compressed until its porosity reached 0.40, and the size of the simulation cell was 86.3 × 83.6 × 78.8 Å.
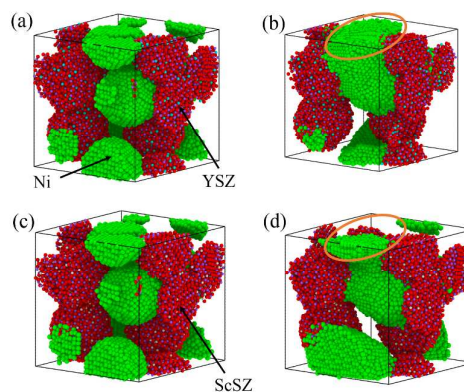

Figure 2. Time evolution of the Ni/YSZ and Ni/ScSZ multi-nanoparticle models. (a) and (c) are the initial structure of the Ni/YSZ and Ni/ScSZ nanoparticles. (b) and (c) are the sintering of Ni nanoparticles in Ni/YSZ and Ni/ScSZ multi-nanoparticle models at 500 ps.
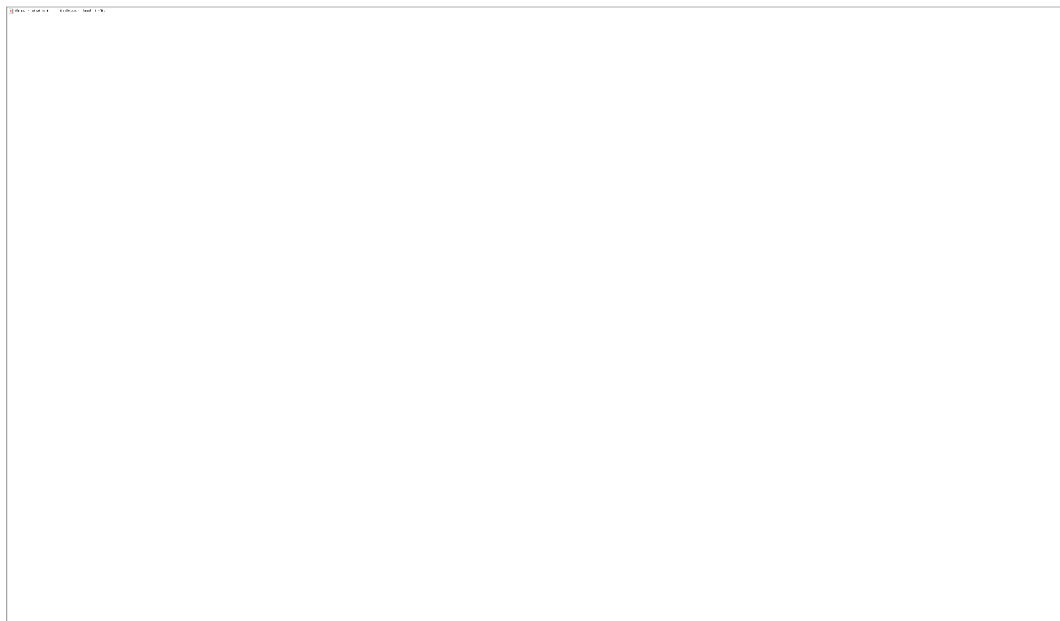
Figure 3. Cross-sectional snapshots of the time evolution of the Ni/YSZ ((a)–(d)) and Ni/ScSZ ((e)–(h)) multi-nanoparticle models with a porosity of 0.40 at 1073 K: (a) and (e) t = 0 ps, (b) and (f) t = 4 ps, (c) and (g) t = 9 ps, and (d) and (h) t = 500 ps.

multi-nanoparticles (Figure 2(a)). Figure 2(d) is the Ni/ScSZ multi-nanoparticle structure after the sintering simulation. The Ni nanoparticles shown by the orange circle in Figure 2(d) do not sinter, which is different from the sintering process in Ni/YSZ multi-nanoparticle model (Figure 2(b)). Thus, we suggest different sintering processes in Ni/YSZ and Ni/ScSZ multi-nanoparticle models. Then, to reveal the details of the sintering process in Ni/YSZ and Ni/ScSZ multi-nanoparticle models, we examined the cross-sectional snapshots of the sintering process of Ni/YSZ and Ni/ScSZ multi-nanoparticle models. Figure 3 shows cross-sectional snapshots of the sintering of Ni nanoparticles in the Ni/YSZ ((a)–(d)) and Ni/ScSZ ((e)–(h)) multi-nanoparticle models at 0, 4, 9, and 500 ps, respectively. The top left, middle left, and middle right Ni nanoparticles in Figure 3(a)–(d) are called Nos. 1, 2, and 3, and those in Figure 3(e)–(h) are called Nos. 4, 5, and 6. In Figure 3(a), there are three Ni nanoparticles (Nos. 1–3) and two YSZ nanoparticles. Ni nanoparticles Nos. 1 and 2, and Nos. 2 and 3 are attracted to each other in the Ni/YSZ multi-nanoparticle model (Figure 3(b)). This mutual attraction was also observed in previous MD sintering simulations of two titanium oxide nanoparticles without a substrate[19,20] and of two palladium nanoparticles on a MgO(001) substrate[17] during the initial stage. At 4 ps, nanoparticles Nos. 1 and 2 make contact (Figure 3(b)), indicating that sintering occurs between Nos. 1 and 2. Then, No. 1 keeps moving toward No. 2 on the YSZ surface and the contact area between them grows (Figure 3(c)). In addition, at 9 ps, Nos. 2 and 3 make contact with each other through the interspace between the two YSZ nanoparticles, which corresponds to a pore in the YSZ framework structure (Figure 3(c)). Nos. 2 and 3 keep moving toward each other and the contact area between them also grows (Figure 3(d)). The three Ni nanoparticles finally form one compact nanoparticle at 500 ps, whereas the YSZ nanoparticles are almost

unchanged (Figure 3(d)). By using a microscope equipped with a high-resolution digital camera and an imaging system, Simwonis et al.[34] observed that the Ni particles coalesce and YSZ particles do not change in a Ni/YSZ anode after sintering. Our results from the multi-nanoparticle sintering simulation agree with these experimental observations. Therefore, our sintering simulation with the multi-nanoparticle model successfully reproduces the sintering process in the porous structure. Figure 3(e) is the initial Ni/ScSZ multi-nanoparticle model, showing the location of the nanoparticles, similar to that in the Ni/YSZ multi-nanoparticle model (Figure 3(a)). At 4 ps, Ni nanoparticles Nos. 5 and 6 approach each other through the pore in the ScSZ framework structure (Figure 3(f)). Ni nanoparticles Nos. 4 and 5 do not approach each other, and do not make contact at 4 ps in the Ni/ScSZ multi-nanoparticle
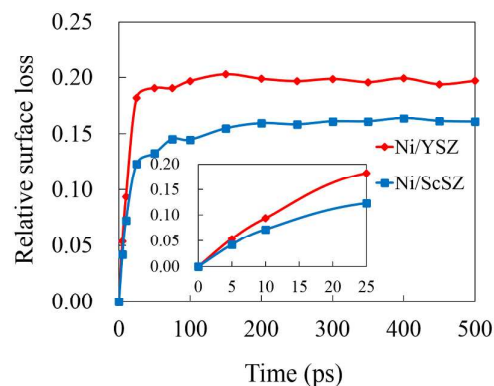

Figure 4. Time evolution of the relative surface loss at 1073 K in the Ni/YSZ and Ni/ScSZ multi-nanoparticle models.

model. However, nanoparticles Nos. 1 and 2 make contact at 4 ps in the Ni/YSZ multi-nanoparticle model (Figure 3 (b)). This indicates that the mutual movement between the Ni nanoparticles in the Ni/YSZ multi-nanoparticle model is faster than that in the Ni/ScSZ multi-nanoparticle model. At 9 ps, Nos. 5 and 6 make contact with each other (Figure 3(g)). This indicates that the sintering between Nos. 5 and 6 takes place from 9 ps. In contrast, Nos. 4 and 5 do not approach each other. Nos. 5 and 6 keep moving toward each other through the pore between ScSZ nanoparticles and the contact area between them grows. At 500 ps, Nos. 5 and 6 form one compact nanoparticle due to the sintering (Figure 3(h)). The sintering of Nos. 4 and 5 does not happen in the Ni/ScSZ multi-nanoparticle model (circle in Figure 3(h)), whereas Nos. 1 and 2 are sintered in the Ni/YSZ multi-nanoparticle model (circle in Figure 3(d)). This result suggests that the degree of sintering of the Ni nanoparticles in the Ni/YSZ anode is larger than that in the Ni/ScSZ anode. Remarkably, Ni nanoparticle No. 4 adheres to its neighboring ScSZ nanoparticle (dashed circle in Figure 3(h)). This adhesion was not found at 0 ps (Figure 3(e)). The adhesion of Ni nanoparticle No. 1 to its neighboring YSZ nanoparticle is not observed in the Ni/YSZ model (Figure 3(d)). Thus, Ni nanoparticles Nos. 1–3 were sintered in the Ni/YSZ porous structure, whereas only Nos. 5 and 6 were sintered in the Ni/ScSZ porous structure.

Experimentally, there is a progressive decrease of surface area of Ni nanoparticles during the sintering.[35] To quantify the sintering processes of Ni nanoparticles in the Ni/YSZ and Ni/ScSZ models, we estimated the decrease in surface area of the Ni nanoparticles during sintering. We calculated the relative surface loss, as defined by $(S_0 - S_t)/S_0$, where S_0 and S_t are the total surface area of the Ni nanoparticles at 0 and t ps, respectively. Here, we defined the surface area of the Ni nanoparticles in contact with the gas phase as the adsorption surface area of the Ni nanoparticles, and we defined the surface area of the Ni nanoparticles in contact with the ceramic nanoparticles (YSZ and ScSZ) as the Ni-ceramic interfacial area. The total surface area of the Ni nanoparticles corresponds to the sum of the adsorption surface area of the Ni nanoparticles and the Ni-ceramic interfacial area; this was calculated according to the Meyer method.[36] In the Meyer method, the simulation cell is divided into small mesh grids by a length of 0.1 Å. The grids within the van der Waals radius are defined as nanoparticle interior grids. The van der Waals radii for Ni, O, Zr, Y, and Sc are 1.63, 1.52, 1.96, 2.20, and 1.98 Å, respectively.[37] The grids in contact with the nanoparticle interior grids are defined as surface grids and used for calculating the surface area (S_t). The other grids are defined as gas phase grids. Figure 4 shows the time evolution of the decrease of the relative total surface area of Ni nanoparticles. The relative surface loss shows a rapid increase during the sintering in the initial stage (~25 ps) in both Ni/YSZ and Ni/ScSZ multi-nanoparticle models, indicating that sintering happens. The relative surface loss in Ni/ScSZ is smaller than that in Ni/YSZ at the beginning of the sintering simulation (inset, Figure 4). At 500 ps, the relative surface losses in Ni/YSZ and Ni/ScSZ are 0.20 and 0.16, respectively. Thus, the degree of sintering in the Ni/YSZ anode is larger than that in the Ni/ScSZ anode in our simulations. The previous sintering studies by MD simulations[18,19,38,39] suggested that the sintering of nanoparticles occurs within 500 ps. In this study, we observed the sintering process in our multi-nanoparticle models within a

few hundred ps. This is similar to the previous sintering studies by MD simulations. Furthermore, B. C. Kim et al. showed that decrease in nanoparticle size in nano-sized powder regime promoted the sintering process by experiment.[40] We calculated the Ni/YSZ and Ni/ScSZ multi-nanoparticle models with nanoparticle of 48 Å at 0.4 porosity in order to discuss the effect of the nanoparticle size on the sintering process. The relative surface loss increases in both Ni/YSZ and Ni/ScSZ multi-nanoparticle models at the initial stage (Figure S4), indicating that the sintering occurs. Then, the relative surface loss shows little change after the 200 ps. In Figure 4, the increase in relative surface loss is very fast and the relative surface loss shows little change after 25 ps. Thus, the sintering process in the model with nanoparticles of 48 Å is slowed down compared to that with nanoparticles of 40 Å, which is in good agreement with the previous sintering simulation results by MD.[18,19,38,39] The relative surface losses in Ni/YSZ and Ni/ScSZ are 0.20 and 0.15, respectively, at 500 ps (Figure S4). Thus, the degree of the sintering in Ni/ScSZ is smaller than that in Ni/YSZ model, which is consistent with the results in the models with nanoparticles of 40 Å. Furthermore, several previous studies investigated the effect of the nanoparticle size on the sintering by using MD simulations.[18,19,38,39] They showed that increasing the nanoparticle size does not change the sintering process. Our result is in good agreement with the previous results. Therefore, we conclude that the change of the nanoparticle size does not affect our sintering simulation results.

To inhibit sintering in the anode during SOFC operation, the mechanism for the difference in the sintering processes in
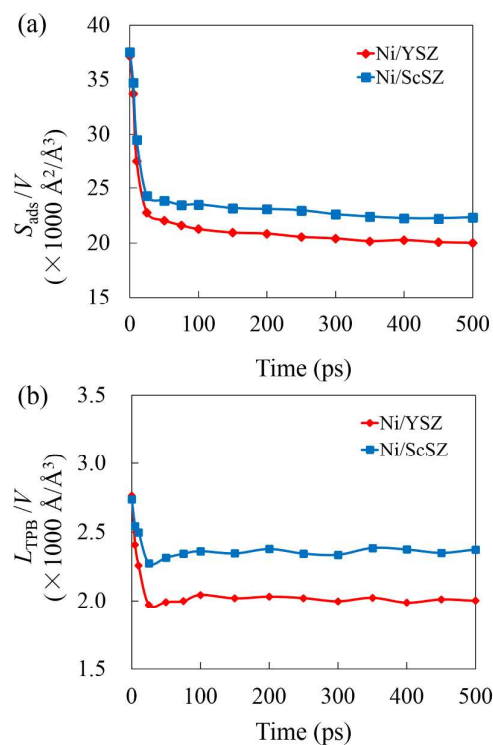

Figure 5. Time evolution of (a) the adsorption surface area of Ni nanoparticles and (b) the TPB length in the Ni/YSZ and Ni/ScSZ multi-nanoparticle models at 1073 K.

ARTICLE

Ni/YSZ and Ni/ScSZ must be determined. As shown in Table 3, the DFT-based interaction parameter between Ni and Sc is larger than that between Ni and Y. Thus, the attractive interaction between the Ni and the ScSZ surface is stronger than that between the Ni and the YSZ surface. Previous experimental studies that used a temperature-programmed reduction technique revealed that the interaction between Ni and ScSZ is larger than that between Ni and YSZ.[41,42] Our result agrees well with these studies. Ni nanoparticles strongly adhere to ScSZ nanoparticles because of the strong attractive interaction, decreasing the movement of Ni nanoparticles on the surface of ScSZ nanoparticles, as compared with YSZ nanoparticles (Figures 4(b) and (f)). As shown in Figure 3(h), Ni nanoparticle No. 4 prefers to make contact with the neighboring ScSZ nanoparticles because of the strong attractive interaction between Ni and ScSZ in the Ni/ScSZ multi-nanoparticle model (dashed circle in Figure 3(h)). It prevents Ni nanoparticle No. 4 from making contact with No. 5 in the Ni/ScSZ multi-nanoparticle model, which suppresses the sintering in the Ni/ScSZ anode (Figures 4(d) and (h)). The sintering process is affected by the strength of the attractive interaction between Ni and the ceramic (YSZ and ScSZ). We performed sintering simulations of five different initial nanoparticle arrangements with the Ni/YSZ and Ni/ScSZ multi-nanoparticle models to confirm the repeatability of the simulation. Comparing the sintering simulation results for the Ni/YSZ and Ni/ScSZ multi-nanoparticle models showed that in the Ni/ScSZ models, the movement of Ni nanoparticles was decreased and sintering was suppressed in all five simulations because of the strong adhesion of Ni nanoparticles to the neighboring ScSZ nanoparticles. Our results show that increasing the attractive interaction between Ni and ceramic decreases the sintering in the Ni/ceramic porous structure. Thus, our multi-nanoparticle sintering simulation method reveals the effect of the ceramic type on the sintering of Ni nanoparticles, and is suitable for use in designing ceramics intended to inhibit the sintering of Ni nanoparticles in the anode.

In the Ni-based cermet anode, the hydrogen fuel adsorbs and dissociates on the surface of the Ni nanoparticles. The dissociated hydrogen atoms diffuse and reach the triple phase boundary (TPB) of the gas phase (hydrogen fuel), Ni phase, and ceramic phase. Next, the hydrogen atoms react with the oxygen ions from the electrolyte during SOFC operation. Greater numbers of hydrogen adsorption sites increase the electrochemical reaction. Moreover, the electrochemical reaction in the anode occurs at the TPB only. Thus, the adsorption surface area of the Ni nanoparticles and the length of the TPB play an important role in the overall performance of SOFCs.[2] To reveal the effect of the sintering on the degradation in the Ni/YSZ and Ni/ScSZ multi-nanoparticle models, we investigated the adsorption surface area of Ni nanoparticles and the length of the TPB in the multi-nanoparticle models. To estimate the adsorption surface area of Ni nanoparticles, we initially calculated surface area by using the Meyer method.[36] The grids of surface area of Ni nanoparticles in contact with the gas phase grids are determined as adsorption surface grids and used for calculating the adsorption surface area (S_{ads}). To compare the adsorption surface area of the Ni nanoparticles in Ni/YSZ and Ni/ScSZ, the adsorption surface area of the Ni nanoparticles was divided by the simulation cell volume (V). Figure 5(a)

shows the time evolution of S_{ads}/V during the sintering simulation in the Ni/YSZ and Ni/ScSZ multi-nanoparticle models. The adsorption surface area decreases drastically during the initial stage of sintering (~25 ps) in both Ni/YSZ and Ni/ScSZ multi-nanoparticle models. Decreasing the adsorption surface area indicates the decrease in the hydrogen adsorption area, showing that sintering degrades the hydrogen adsorption sites. Furthermore, the decrease of the adsorption surface area in Ni/ScSZ is smaller than in Ni/YSZ at 500 ps, because the ceramic type means that the degree of sintering in Ni/ScSZ is smaller than in Ni/YSZ (Figure 4).

Next, we discuss the TPB length, which indicates the number of chemical reaction sites for the hydrogen oxidation. We calculated the surface area by using the Meyer method.[36] The grids belonging to the surface area of the Ni and ceramic nanoparticles simultaneously were defined as overlapping grids. The surface grids of Ni nanoparticles in direct contact with the surface grids of ceramic nanoparticles were defined as contact grids. The overlapping and contact grids in contact with the gas phase grids were determined as TPB grids and were used for calculating the TPB length (L_{TPB}). To compare the TPB length in Ni/YSZ and Ni/ScSZ, the TPB length was divided by the simulation cell volume (V). Figure 5(b) shows the time evolution of L_{TPB}/V. The TPB length shows a rapid decrease during the sintering of Ni nanoparticles at the initial stage (~25 ps) in both the Ni/YSZ and Ni/ScSZ models, which decreases the number of reaction sites for hydrogen oxidation. The anodic reaction activity decreases and the activation overpotential increases during sintering, because the decreasing TPB length increases the activation overpotential.[42] Furthermore, the decrease of TPB length in the Ni/YSZ is larger than that in Ni/ScSZ. This is because the degree of sintering in the Ni/YSZ anode is larger than in the Ni/ScSZ anode (Figure 4). Time evolution of the adsorption surface area and TPB length indicates that the Ni/YSZ anode degrades more than the Ni/ScSZ anode during the Ni nanoparticle sintering. Sumi et al.[9,10] reported that the increase in anode overpotential with operation time was larger for Ni/YSZ than for Ni/ScSZ. Our result agrees well with the experimental results. Therefore, our multi-nanoparticle sintering simulation method models the sintering process and the degradation induced by sintering in porous structures. The results show that the degradation of the adsorption sites and reaction sites depends strongly on the degree of sintering. The strong attractive interaction between the Ni and the ceramic plays an important role in preventing the sintering and the degradation induced by the sintering in the porous anode.

3.2. Effect of Porosity on Sintering in Ni/YSZ and Ni/ScSZ Multi-nanoparticle Models

Several studies showed that the performance and durability of SOFCs are closely related to the anode porosity.[22,23] To inhibit the degradation of SOFCs, it is essential to understand the effect of porosity on the sintering and the degradation induced by sintering in the Ni/YSZ and Ni/ScSZ anodes. In this study, to investigate the effect of porosity on the sintering in Ni/YSZ and Ni/ScSZ anodes, we built Ni/YSZ and Ni/ScSZ multi-nanoparticle models with porosities from 0.05 to 0.65 at intervals of 0.05 based on our developed modeling methodology as described in Section 2. First, we examined the relative surface loss of Ni nanoparticles to quantify the sintering processes of Ni nanoparticles. The relative surface
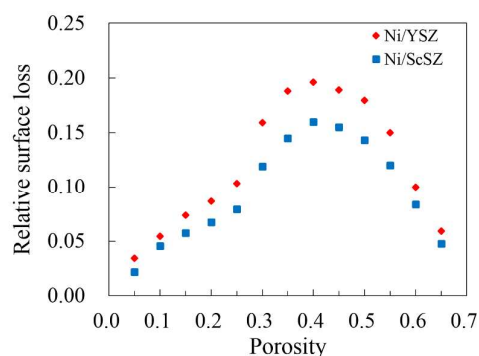
Figure 6. Effect of porosity on surface area loss in the Ni/YSZ and Ni/ScSZ multi-nanoparticles models at 1073 K.

loss was calculated by $(S_0 - S)/S_0$, where S_0 and S are the surface area of Ni nanoparticles at 0 ps and the averaged surface area of Ni nanoparticles from 200 to 500 ps, respectively. This is because we observed little change in the relative surface loss after 200 ps in Figure 4. Figure 6 shows the effect of porosity on the relative surface loss of Ni nanoparticles in Ni/YSZ and Ni/ScSZ multi-nanoparticle models. In the Ni/YSZ models, the relative surface loss increases slightly as the porosity increases from 0.05 to 0.25, and increases sharply above 0.25, reaching a local maximum value at a porosity of 0.40. Subsequently, the relative surface loss decreases with increasing porosity from 0.40 to 0.65. These results indicate that the degree of sintering in the Ni/YSZ model depends on the porosity. Interestingly, small relative surface loss is observed in the Ni/YSZ models with both small and large porosity, indicating that the degree of Ni nanoparticles sintering is small at both small and large porosities. This agrees with our previous study,[25] showing that the sintering is suppressed in the small and large porosity models. When the porosity is smaller than 0.25, the pore size of the YSZ framework decreases with decreasing porosity. The small pores suppress the growth of the contact area between Ni nanoparticles, inhibiting the sintering of the Ni nanoparticles in the Ni/YSZ model with the small porosity. As the porosity increases from 0.25 to 0.40, the relative surface loss increases owing to the growth of the contact area between Ni nanoparticles in pores that are sufficiently large. When the porosity is larger than 0.40, the relative surface loss decreases with the increase in porosity. This is because the large porosity increases the distance between Ni nanoparticles and prevents the Ni nanoparticles from making contact. Interestingly, this mechanism of inhibiting sintering at large porosities is different from that at small porosities. In the Ni/ScSZ multi-nanoparticle models with a porosity from 0.05 to 0.65, we observed similar variations in relative surface loss with the porosity. Nevertheless, the relative surface loss in Ni/ScSZ is smaller than that in Ni/YSZ at each porosity. This is because the effect of the ceramic type causes different sintering behavior in Ni/YSZ and Ni/ScSZ (see Section 3.1). The strong attractive interaction between Ni and ScSZ compared with that between Ni and YSZ decreases the movement of Ni nanoparticles. This suggests that ScSZ decreases the degree of sintering. Furthermore, an interesting phenomenon is that the

difference in the relative surface loss between the Ni/ScSZ and Ni/YSZ models increases from a porosity of 0.05 to 0.40, and then decreases from a porosity of 0.40 to 0.65 (Figure 6). This indicates that the effect of ceramic type on sintering is affected by the porosity. When the porosity is less than 0.40, Ni nanoparticles cannot move through the small pores easily owing to the suppression of the contact area between Ni nanoparticles in both Ni/YSZ and Ni/ScSZ models. Therefore, the effect of ceramic types is not obvious and the difference in the relative surface loss between the Ni/YSZ and Ni/ScSZ models is small. When the porosity is more than 0.40, the large porosity increases the distance between Ni nanoparticles and prevents the Ni nanoparticles from making contact. The ceramic type has a negligible effect when the model porosity is large. These phenomena cannot be observed in the conventional two- or three-nanoparticle model.[18–20] We performed sintering simulations with three different initial nanoparticle configurations at each porosity to confirm the repeatability of the simulations. The sintering depended on the porosity in all the Ni/ScSZ and Ni/YSZ models. Thus, the porosity plays an important role in preventing sintering.

The effect of the porosity on the degradation of the adsorption sites and the chemical reaction sites was examined by calculating the adsorption surface area of Ni nanoparticles and TPB length before and after sintering in the Ni/YSZ and Ni/ScSZ models with porosities of 0.05–0.65. To compare the adsorption surface area and TPB length in the Ni/YSZ and Ni/ScSZ models, the adsorption surface area (S_{ads}) and TPB length (L_{TPB}) were divided by the simulation cell volume (V). The adsorption surface area and the TPB length before the sintering were calculated from the initial Ni/YSZ and Ni/ScSZ models. The adsorption surface area and the TPB length after the sintering were obtained by calculating the average values of the adsorption surface area and the TPB length from 200 to 500 ps, because the change in the adsorption surface area and TPB length after 200 ps was small (Figures 6(a) and (b)). Figures 8(a) and (b) show the average values of S_{ads}/V and L_{TPB}/V obtained from sintering simulations with three initial nanoparticle arrangements at each porosity. Figure 7(a) shows the dependence of S_{ads}/V on the porosity in the Ni/YSZ and Ni/ScSZ multi-nanoparticle models. In all Ni/YSZ models, the initial adsorption surface area increases from a porosity of 0.05 to 0.40, and then decreases from a porosity of 0.40 to 0.65. After sintering, the adsorption surface area decreases in all Ni/YSZ models with the porosity from 0.05 to 0.65. This result indicates that the sintering degraded the adsorption sites. The decrease of the adsorption surface area increases slowly from a porosity of 0.05 to 0.25, increases sharply from 0.25 to 0.40, and then decreases from 0.40 to 0.65. In all Ni/ScSZ models with porosities from 0.05 to 0.65, the decrease in the adsorption surface area with increasing porosity after sintering is similar to that in Ni/YSZ models. In addition, the decrease of adsorption surface area in Ni/ScSZ models is smaller than that in the Ni/YSZ models at all porosities. After sintering, the difference in the decrease of the adsorption surface area between Ni/YSZ and Ni/ScSZ increases at porosities from 0.05 to 0.40, and then decreases at porosities from 0.40 to 0.65. These results indicate that the decrease of the adsorption surface area corresponds to the degree of sintering.

Figure 7(b) shows the dependence of L_{TPB}/V on the porosity in the Ni/YSZ and Ni/ScSZ models. In all Ni/YSZ models, the initial TPB length increases from a porosity of 0.05 to 0.25, and
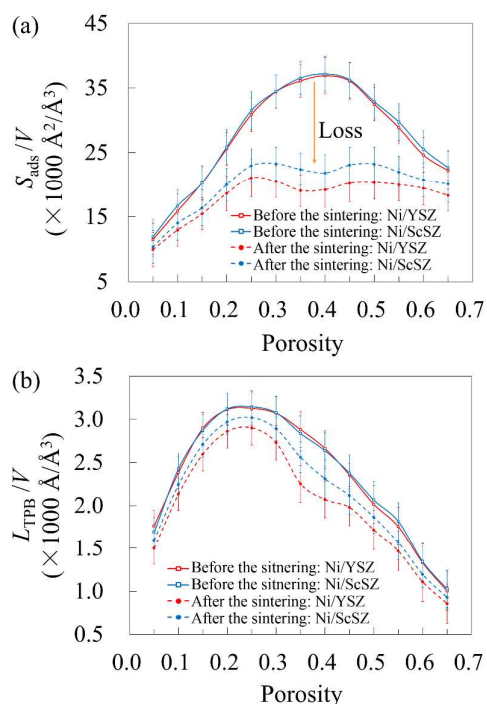
Figure 7. Changes in the (a) adsorption surface area of Ni nanoparticles and (b) TPB length as a function of the porosity in the Ni/YSZ and Ni/ScSZ multi-nanoparticles models. The averaged data with the error bars for three simulation runs of the Ni/YSZ and Ni/ScSZ multi-nanoparticle models at each porosity are shown.

then decreases from a porosity of 0.25 to 0.65. In all Ni/YSZ models, the TPB length decreases after the sintering with the porosity from 0.05 to 0.65 (Figure 7(b)). In the Ni/YSZ models, the decrease of the TPB length slightly increases with porosity from 0.05 to 0.25 and increases sharply from a porosity of 0.25 to 0.40. Then, it decreases in the Ni/YSZ models with the porosity from 0.40 to 0.65. In all Ni/ScSZ models with porosities from 0.05 to 0.65, we also observed a similar decrease in TPB length with porosity after sintering. In addition, the decrease in TPB length in Ni/ScSZ is smaller than that in Ni/YSZ at each porosity due to the effect of ceramic type. The difference in the decrease of TPB length between the Ni/YSZ and Ni/ScSZ models increases from a porosity of 0.05 to 0.40, and then decreases from a porosity of 0.40 to 0.65. These results indicate that the decrease in the TPB length depends on the degree of sintering in the Ni/YSZ and Ni/ScSZ anodes. In addition, the error bars in Figure 7(a) and (b) include the effects of the different positions of nanoparticles and the different interfaces between Ni and the different ceramic (YSZ and ScSZ) surfaces in three different initial models at each porosity. Even though the error in Figure 7(a) and (b) is considered, the degree of the sintering and the degradation in Ni/ScSZ models are smaller than those in Ni/YSZ models at all porosities. The effect of the surface structures of ceramic nanoparticles does not affect our conclusions. Furthermore, Figure 7(a) shows two local maximum adsorption surface areas at porosities of 0.25 and 0.50 after sintering. Meanwhile, a maximum TPB length is observed at a porosity of

0.25 after sintering (Figure 7(b)). Our simulation shows large adsorption and reaction sites at a porosity of 0.25 after sintering. Thus, our multi-nanoparticle sintering MD simulation can be used to optimize the anode porosity to obtain high-performance anodes after sintering. These results obtained with our multi-nanoparticle sintering simulation method cannot be obtained in conventional two- or three-nanoparticle models,[18-20] which cannot consider the effect of the porous structure. Furthermore, the decrease in the number of adsorption and reaction sites in Ni/ScSZ is larger than in Ni/YSZ at all porosities after sintering. Thus, we showed theoretically that degradation in the ScSZ anode is inhibited compared with the YSZ anode after sintering.
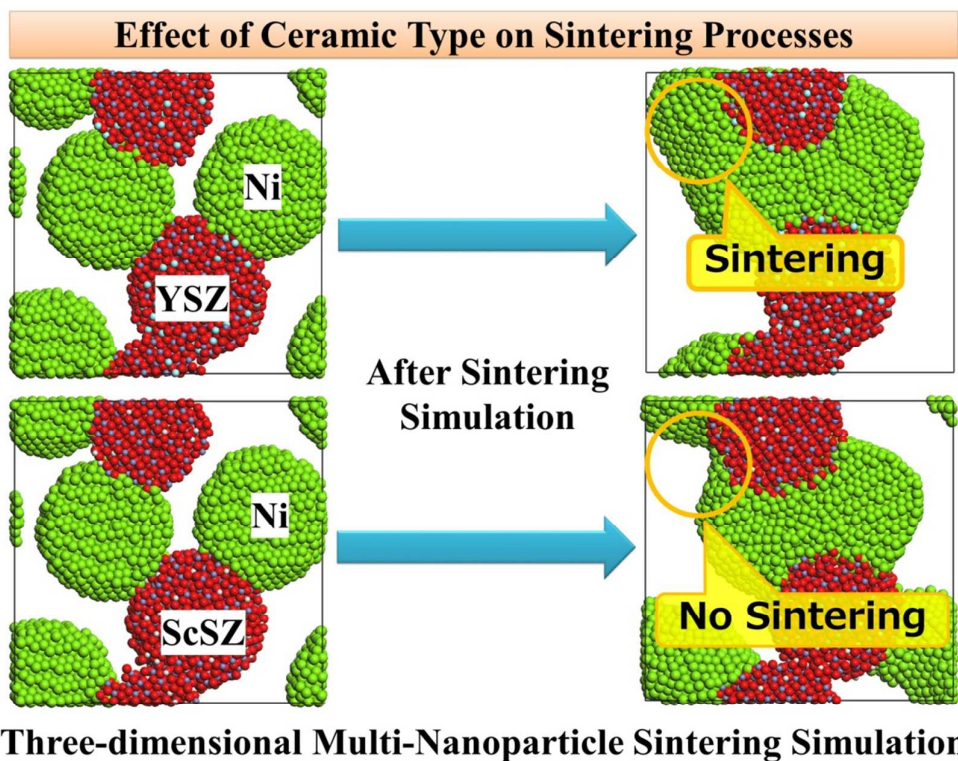
4. Conclusion

The sintering and the degradation in the Ni/YSZ and Ni/ScSZ anodes were studied by using our multi-nanoparticle sintering simulation based on MD. First, we used our Ni/YSZ and Ni/ScSZ multi-nanoparticle models to determine the effect of the ceramic type (YSZ and ScSZ) on the sintering. During the sintering simulations, Ni nanoparticles approach each other on the YSZ and ScSZ nanoparticle surfaces. The Ni nanoparticles make contact with each other and sintering of the Ni nanoparticles occurs. The movement of Ni nanoparticles on the ScSZ nanoparticle surfaces is smaller in the Ni/ScSZ model than in Ni/YSZ model because the attractive interaction between Ni and ScSZ is stronger than between Ni and YSZ resulting in the strong adhesion of Ni nanoparticles to the ScSZ nanoparticles. The strong adhesion of Ni nanoparticles to ScSZ prevents the Ni nanoparticles from approaching each other in Ni/ScSZ, suppressing the sintering in Ni/ScSZ. Our multi-nanoparticle sintering MD simulations revealed the different sintering processes of Ni nanoparticles in Ni/YSZ and Ni/ScSZ anodes, which could not be revealed by conventional two- or three-nanoparticle sintering MD simulations. Next, to elucidate the effect of the sintering on the degradation, we discussed the changes in the adsorption surface area of the Ni nanoparticles and the TPB length in the Ni/YSZ and Ni/ScSZ multi-nanoparticle models. The adsorption surface areas of Ni nanoparticles and TPB length decrease with an increase in the degree of the sintering in the Ni/YSZ and Ni/ScSZ models. We revealed that the decrease in the adsorption surface area and TPB length in the Ni/YSZ is larger than that in Ni/ScSZ. Our multi-nanoparticle sintering MD simulations provides an analysis of the adsorption surface area and TPB length in the porous anode. We examined the effect of the porosity on the sintering and the degradation induced by the sintering in the Ni/YSZ and Ni/ScSZ models. The degree of sintering depends on the porosity in both the Ni/YSZ and Ni/ScSZ models. Furthermore, the decrease of the adsorption surface area and TPB length depended on the degree of sintering. After sintering, the two local maximum adsorption surface areas are at porosities of 0.25 and 0.50, and the maximum TPB length is at a porosity of 0.25. Our simulation shows strong adsorption and a large number of reaction sites at a porosity of 0.25 after sintering. Thus, our multi-nanoparticle sintering MD simulation can be used to optimize the anode porosity to obtain high-performance anodes after sintering. Furthermore, the decrease in the number of the adsorption and reaction sites in Ni/ScSZ is larger than in Ni/YSZ at each porosity after sintering. Our results show theoretically that using ScSZ in the anode

instead of YSZ inhibits the degradation of anode after sintering. We expect that this study will provide a theoretical basis for designing durable porous anodes.

Notes and references

1 S. Singhal, *Solid State Ionics*, 2000, **135**, 305–313.
2 R. M. Ormerod, *Chem. Soc. Rev.*, 2003, **32**, 17–28.
3 D. J. L. Brett, A. Atkinson, N. P. Brandon and S. J. Skinner, *Chem. Soc. Rev.*, 2008, **37**, 1568–1578.
4 E. D. Wachsman and K. T. Lee, *Science*, 2011, **334**, 935–939.
5 S. P. Jiang, *J. Mater. Sci.*, 2003, **38**, 3775–3782.
6 A. Faes, A. Hessler-Wyser, D. Presvytes, C. G. Vayenas and H. J. Van, *Fuel Cells*, 2009, **9**, 841–851.
7 H. Itoh, T. Yamamoto, M. Mori, T. Abe, *Proceedings of the Fourth International Symposium on Solid Oxide Fuel Cells (SOFC-IV)*, ed. M. Dokiya, O. Yamamoto, H. Tagawa, and S. C. Singhal, The Electrochem. Soc., Yokohama, Japan, 1995, pp. 18-23.
8 H. Kishimoto, K. Yamaji, T. Horita, Y. P. Xiong, N. Sakai, M. E. Brito and H. Yokokawa, *J. Electrochem. Soc.*, 2006, **153**, A982–A988.
9 H. Sumi, K. Ukai, Y. Mizutani, H. Mori, C. Wen, H. Takahashi and O. Yamamoto, *Solid State Ionics*, 2004, **174**, 151–156.
10 H. Sumi, Y. H. Lee, H. Muroyama, T. Matsui and K. Eguchi, *J. Electrochem. Soc.*, 2010, **157**, B1118–B1125.
11 M. J. D. Rushton, A. Chroneos, S. J. Skinner, J. A. Kilner and R. W. Grimes, *Solid State Ionics*, 2013, **230**, 37–42.
12 C. Chen, D. Chen, Y. Gao, Z. Shao and F. Ciucci, *J. Mater. Chem. A*, 2014, **2**, 14154.
13 A. Tarancón, M. Burriel, J. Santiso, S. J. Skinner and J. A. Kilner, *J. Mater. Chem.*, 2010, **20**, 3799.
14 W. Araki, Y. Imai and T. Adachi, *J. Eur. Ceram. Soc.*, 2009, **29**, 2275–2279.
15 M. Kilo, C. Argirusis, G. Borchardt and R. A. Jackson, *Phys. Chem. Chem. Phys.*, 2003, **5**, 2219.
16 P. K. Schelling, S. R. Phillpot and D. Wolf, *J. Am. Ceram. Soc.*, 2001, **84**, 1609–1619.
17 A. Miyamoto, R. Yamauchi and M. Kubo, *Appl. Surf. Sci.*, 1994, **75**, 51–57.
18 H. Zhu, *Philos. Mag. Lett.*, 1996, **73**, 27–33.
19 V. N. Koparde and P. T. Cummings, *J. Phys. Chem. B*, 2005, **109**, 24280–24287.
20 B. Buesser, A. J. Gröhn and S. E. Pratsinis, *J. Phys. Chem. C*, 2011, **115**, 11030–11035.
21 T. Hawa and M. Zachariah, *Phys. Rev. B*, 2007, **76**, 054109.
22 M. Pihlatie, T. Ramos and A. Kaiser, *J. Power Sources*, 2009, **193**, 322–330.
23 J. H. Yu, G. W. Park, S. Lee and S. K. Woo, *J. Power Sources*, 2007, **163**, 926–932.
24 J. Xu, R. Sakanoi, Y. Higuchi, N. Ozawa, K. Sato, T. Hashida and M. Kubo, *J. Phys. Chem. C*, 2013, **117**, 9663–9672.
25 J. Xu, Y. Higuchi, N. Ozawa, K. Sato, T. Hashida and M. Kubo, *ECS Trans.*, 2013, **57**, 2459–2464.
26 M. Yoshimoto, T. Maeda, T. Ohnishi, H. Koinuma, O. Ishiyama, M. Shinohara, M. Kubo, R. Miura and A. Miyamoto, *Appl. Phys. Lett.*, 1995, **67**, 2615–2617.
27 L. Verlet, *Phys. Rev.*, 1967, **159**, 98–103.
28 K. Suzuki, M. Kubo, Y. Oumi, R. Miura, H. Takaba, A. Fahmi, A. Chatterjee, K. Teraishi and A. Miyamoto, *Appl. Phys. Lett.*, 1998, **73**, 1502–1504.
29 L. Girifalco and V. Weizer, *Phys. Rev.*, 1959, **114**, 687–690.
30 F. Yuan and X. Wu, *Comput. Mater. Sci.*, 2014, **85**, 8–15.
31 F. Yuan, L. Chen, P. Jiang, X. Wu, and X. Wu, *J. Appl. Phys.*, 2014, **115**, 063509.
32 N. Gunkelmann, D. R. Tramontina, E. M. Bringa and H. M. Urbassek, *J. Appl. Phys.*, 2015, **117**, 085901.
33 S. Primdahl, M. Mogensen, *J. Electrochem. Soc.*, 1999, **146**, 2827–2833.
34 D. Simwonis, F. Tietz, O. Stöver, *Solid State Ionics*, 2000, **132**, 241–251.
35 T. J. Gray, *J. Am. Ceram. Soc.*, 1954, **37**, 534–538.
36 A. Y. Meyer, *J. Comput. Chem.*, 1988, **9**, 18–24.
37 S. S. Batsanov, *Inorg. Mater.*, 2001, **37**, 871–885.
38 J. S. Raut, R. B. Bhagat and K. A. Fichthorn, *Nanostructured Mater.*, 1998, **10**, 837–851.
39 V. N. Koparde and P. T. Cummings, *J. Nanoparticle Res.*, 2008, **10**, 1169–1182.
40 B. Kim, J. Lee, J. Kim and T. Ikegami, 2002, *Mater. Lett.*, 2002, **114**, 114–119.
41 H. Mori, C. Wen, J. Otomo, K. Eguchi and H. Takahashi, *Appl. Catal. A Gen.*, 2003, **245**, 79–85.
42 H. Sumi, P. Puengjinda, H. Muroyama, T. Matsui and K. Eguchi, *J. Power Sources*, 2011, **196**, 6048–6054.

Table of Contents

The effects of the ceramic type and porosity on the sintering and degradation in Ni/YSZ and Ni/ScSZ anodes are unveiled by recently developed multi-nanoparticle sintering simulation method based on molecular dynamics simulation.